

An Insight Into Neurodegeneration: Harnessing Functional MRI Connectivity in the Diagnosis of Mild Cognitive Impairment

Shuning Han^{1,2}^a, Zhe Sun^{2,3}^b, Kanhao Zhao⁴^c, Feng Duan⁵^d, Cesar F. Caiafa⁶^e,
Yu Zhang^{4,7}^f and Jordi Solé-Casals^{1,8}^g

¹Data and Signal Processing Research Group, University of Vic-Central University of Catalonia, Vic, 08500, Catalonia, Spain

²Image Processing Research Group, RIKEN Center for Advanced Photonics, Riken, Wako-Shi, Saitama, Japan

³Faculty of Health Data Science, Juntendo University, Urayasu, Chiba, Japan

⁴Department of Bioengineering, Lehigh University, Bethlehem, PA 18015, U.S.A.

⁵Tianjin Key Laboratory of Brain Science and Intelligent Rehabilitation, Nankai University, Tianjin, China

⁶Instituto Argentino de Radioastronomía-CCT La Plata, CONICET/ CIC-PBA/ UNLP, V. Elisa 1894, Argentina

⁷Department of Electrical and Computer Engineering, Lehigh University, Bethlehem, PA 18015, U.S.A.

⁸Department of Psychiatry, University of Cambridge, Cambridge CB20SZ, U.K.


fi


Keywords: Alzheimer's Disease, Mild Cognitive Impairment, Graph Convolutional Network, Functional Magnetic Resonance Imaging Analysis, Functional Connectivity.


Abstract: Alzheimer's disease is a progressive form of memory loss that worsens over time. Detecting it early, when memory issues are mild, is crucial for effective interventions. Recent advancements in computer technology, specifically Graph Convolutional Networks (GCNs), have proven to be powerful tools for analyzing Magnetic Resonance Imaging (MRI) data comprehensively. In this study, we developed a GCN framework for diagnosing mild cognitive impairment (MCI) by examining the functional connectivity (FC) derived from resting-state functional MRI (rfMRI) data. Our research systematically explored various types and processing methods of FC, evaluating their performance on the OASIS-3 dataset. The experimental results revealed several key findings. On the one hand, the proposed GCN exhibited significantly superior performance over both the baseline GCN and the Support Vector Machine (SVM) models, with statistically significant differences. It attained the highest average accuracy of 80.3% and a peak accuracy of 88.2%. On the other hand, the GCN framework obtained using individual FCs showed overall slightly better performance than the one using global FCs. However, it is important to note that GCNs using global networks with appropriate connectivity can achieve comparable or even better performance than individual networks in certain cases. Finally, our results also indicate that the connectivity within specific brain regions, such as VIS, DMN, SMN, VAN, and FPC, may play a more significant role in GCN-based MRI classification for MCI diagnosis. These findings significantly contribute to the understanding of neurodegenerative disorders and offer valuable insights into the diverse applications of GCNs in brain analysis and disease detection.


1 INTRODUCTION


Alzheimer's disease (AD) is a progressive neurodegenerative dementia Srivastava et al. (2021). The typical progression of AD comprises three stages: (early) mild cognitive impairment (MCI), moderate dementia, and severe dementia. Detecting patients in the MCI stage is crucial, as it facilitates the implementation of effective interventions to prevent further deterioration of dementia.


^a <https://orcid.org/0009-0004-0792-5484>


^b <https://orcid.org/0000-0002-6531-0769>

^c <https://orcid.org/0000-0002-2955-0917>

^d <https://orcid.org/0000-0002-2179-2460>

^e <https://orcid.org/0000-0001-5437-6095>

^f <https://orcid.org/0000-0003-4087-6544>

^g <https://orcid.org/0000-0002-6534-1979>

Due to the intricate nature of data from various imaging modalities and the organisational complexity of the human brain network, promising advances have been observed in modelling the interactions between various brain regions. This progress is in part due to new learning techniques that rely on graphs derived from image data, apply graph regularisations to the data, and employ graph embedding to represent graphs derived from recorded data. These methods show potential for capturing the fusion of information between networks from different brain imaging modalities, modelling latent spaces within high-dimensional brain networks, and quantifying neuro-biomarkers based on topological features (Liu et al., 2022).

In recent years, research on magnetic resonance imaging (MRI) has significantly contributed to our comprehension of neuropathological mechanisms underlying dementia and its clinical diagnosis (Chandra et al., 2019). Functional MRI (fMRI) furnishes valuable insights with a relatively high spatial resolution (2mm isotropic) and medium temporal resolution (minutes) (Liu et al., 2015). fMRI can be categorized into two types: task-evoked fMRI (tfMRI), collected while the subject is engaged in tasks, and resting-state fMRI (rfMRI), collected during periods of rest. Even in the resting state, spatial patterns of spontaneous neural activities and metabolism persist in the brain. The functional connectivity (FC) between various brain regions can be inferred (Bi et al., 2020). FC serves as a reflection of the brain's functional organization, and alterations in it are believed to be associated with psychiatric disorders (Bullmore and Sporns, 2009).

Recently, the integration of graph theory and machine learning techniques has found extensive application in neuroscience for the analysis of the brain and the detection of diseases (Bi et al., 2020). A novel domain of geometric deep learning, graph neural networks (GNNs), has emerged, which offers the capability to effectively process signals within the non-Euclidean geometry of graphs. Notably, an increasing number of GNNs have been introduced and employed in the analysis of brain MRI and the detection of disorders (Scarselli et al., 2008). For instance, a graph empirical mode decomposition-based data augmentation was presented in (Chen et al., 2022) to generate more samples in small datasets. Parisot et al. (2017) introduced the graph convolution network (GCN) combining fMRI with non-imaging data for brain analysis and disease diagnosis. Wang et al. (2021) presented a connectivity based GCN architecture for fMRI analysis and applied it to classification of autistic patients from normal controls (NCs).

Tang et al. (2022) proposed a contrastive learning framework with an interpretable hierarchical signed graph representation learning model for brain functional network mining. Qu et al. (2023) proposed a univariate neurodegeneration biomarker based GCN semi-supervised classification framework. Nevertheless, there has been insufficient research dedicated to assessing the influence of various FC on brain analysis results. Moreover, the performance of GCN models in MCI detection still falls short of expectations.

Considering the points mentioned above, this study introduces a state-of-art approach in the realm of neurodegeneration detection using fMRI data. The key highlights of this research are as follows:

A Novel FC Based GCN Framework for MCI Detection: We have designed a novel FC based GCN framework for binary classifications utilizing rfMRI data. The GCN framework is applied for the diagnosis of MCI by classifying the MCI from NCs.

Impact of Different Types of FC: This study places special emphasis on understanding the effects of different FC types and processing methods on the GCN framework's performance. In this paper, FC is regarded as a graph and is considered from two aspects: On one side, we compare the difference of using the global FC matrix obtained from the training data versus the individual specific FC matrices of each rfMRI data. On the other side, we employ different processing methods for the FC matrices, and obtain the k nearest neighbor (k -NN) graph and the threshold graph.

An Insight Into Neurodegeneration: The study delves deeply into the analysis of brain networks including self-network and between-network connectivity. This perspective enhances the clinical relevance of neurodegeneration and impact of this study's findings.

The remainder of this paper is structured as follows: Section 2 provides an overview of the dataset and methods employed. In Section 3, we present the analysis results, which are subsequently discussed in Section 4. Finally, Section 5 concludes this study.

2 MATERIALS AND METHODS

In this section, we initially introduce the dataset for classification and elucidate the label assignment process. Following that, we detail the fMRI acquisition and preprocessing methods, generation of diverse FC, and finally the proposed GCN framework and the baseline methods used for comparison.

2.1 Data

We utilize longitudinal rfMRI series for analysis, categorizing them into *NC* and *MCI* based on the relevant clinical assessments of the participants.

2.1.1 OASIS-3 Dataset

We employ the dataset from the Open Access Series of Imaging Studies (OASIS)-3 (LaMontagne et al., 2019) (<https://www.oasis-brains.org>) to validate our proposed GCN framework. The dataset includes longitudinal fMRI, neuropsychological testing and clinical information for 1098 participants. The clinical dementia rating (CDR) scale is utilized to evaluate the dementia status within the clinical data of OASIS-3: CDR 0 denotes normal cognitive function, CDR 0.5 indicates very mild impairment, CDR 1 signifies mild impairment, and CDR 2 reflects moderate dementia. All participants were required to have a $CDR \leq 1$ in the most recent clinical core assessment, and once a participant reached CDR 2, they were no longer eligible for continued participation in the study.

2.1.2 MRI Scans Labelling

MRI scans can be labeled based on Notably, associated CDR values. Notably, clinical assessments were performed on different days from the neural imaging scans, and the time gap between the MRI scan and clinical assessment may exceed one year in the longitudinal OASIS-3 dataset. In this study, MRI scans are classified into two groups: *NC* and *MCI* based on CDR values. An MRI scan is labeled as *NC*, if all recorded clinical assessment results for the corresponding subject are $CDR = 0$; an MRI scan is labeled as *MCI*, if both preceding and subsequent clinical assessment show $CDR \geq 0.5$. For the purpose of maintaining data balance, 503 *NC* and *MCI* rfMRI samples are used for *MCI* detection, respectively.

2.2 Methods

This part provides a comprehensive exposition on the fMRI acquisition and pre-processing methods, along with the various FC processing methods. Following that, we delve into a detailed description of the proposed GCN framework and the baselines. Finally, we present the specific configurations of the proposed GCN framework.

2.2.1 fMRI Acquisition and Preprocessing

The fMRI data for each subject in each run were acquired in resting state for 6 min (164 volumes) uti-

lizing 16-channel head coil in the scanners. The acquired rfMRI data underwent preprocessing using the fMRIPrep pipeline (Esteban et al., 2019). The T1-weighted (T1w) image underwent intensity correction, skull-stripping, and spatial normalization through nonlinear registration (Avants et al., 2008). Employing FSL, brain features such as cerebrospinal fluid, white matter, and grey matter were segmented from the reference, brain-extracted T1 weighted image (Zhang et al., 2000). The fieldmap information was used to correct distortion in low-frequency and high-frequency components of fieldmap. Subsequently, a corrected echo-planar imaging reference was obtained from a more accurate co-registration with the anatomical reference. The blood-oxygenation-level-dependent (BOLD) reference was then transformed to the T1-weighted image with a boundary-based registration method, configured with nine degrees of freedom to account for distortion remaining in the BOLD reference (Greve and Fischl, 2009). Head-motion parameters were estimated with MCFLIRT (FSL). BOLD signals were slice-time corrected and resampled onto the participant's original space with head-motion correction, susceptibility distortion's correction, and then resampled into standard space, generating a preprocessed BOLD run in MNI152NLin2009cAsym space. Automatic removal of motion artifacts using independent component analysis (ICA-AROMA) (Pruim et al., 2015) was performed on the preprocessed BOLD time-series on MNI space after removal of non-steady-state volumes and spatial smoothing.

2.2.2 FC Construction

The brain FC can be derived from rfMRI and represented as graphs, capturing the statistical time-series correlations between brain regions of interest (ROIs). The preprocessed BOLD-level rfMRI series are averaged into 100 ROIs defined by Schaefer atlas (Schaefer et al., 2018) and subsequently standardized using z-score. Ultimately, the dimension of each fMRI session is 164×100 (100 regions with a length of 164 time samples each). To construct the FC matrices for ROIs, the Pearson correlation coefficient (PCC) is computed between the fMRI time series of every pair of brain regions. Notably, in this study, the diagonal elements of the FC matrices are uniformly set to 0. There are 100 ROIs, resulting in an FC matrix with a shape of 100×100 .

In this paper, we analyse the impact of various types of FC on prediction results, as depicted in Figure 1. The divergence in FC manifests in two dimensions: one is the different FC matrices, individual specific FC matrices obtained from each fMRI data vs.

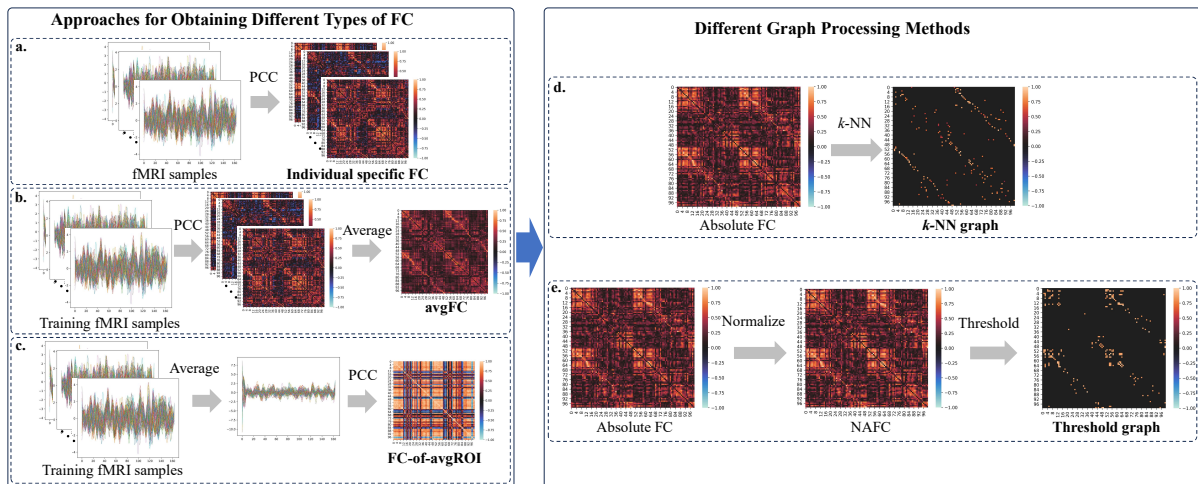


Figure 1: FC construction. Left part: a. Approach for individual specific FC; b. Approach for global **FC-of-avgROI**; c. Approach for global **avgFC**; Right part: d. Method for **k-NN graph**; e. Method for **threshold graph**.

global FC matrix obtained from the training data for both training and testing data; the other is the different processing methods employed to derive the FC matrices. In Han et al. (2024), an extensive and comprehensive analysis is carried out, delving into a wider range of aspects to provide a global understanding. This extended analysis includes the examination of two additional forms of FC, namely top- p and the p -MST (Minimum Spanning Tree). The exploration of these specific types of FC aims to capture a more detailed perspective of the intricate network dynamics within the brain. In addition, the research extends its focus by addressing the classification of at-risk dementia versus normal control subjects. This comparative analysis offers valuable insights into the unique neural signatures associated with this particular condition when contrasted with the normal control group.

- Obtain global FC matrix from training data

Individual specific FC matrices can be derived from each fMRI data by directly computing PCC, as illustrated in Figure 1a. While, a global FC matrix for both training and testing fMRI samples is derived from training samples using distinct approaches. In the first approach for global FC, the **FC-of-avgROI** matrix is obtained from the standardized average data of the training fMRI samples, as illustrated in Figure 1b. In the second approach, we regard the average PCC of all PCC matrices from the training fMRI samples, denoted as **avgFC**, as the global FC matrix, as shown in Figure 1c.

Special to note is that: (i) matrix averaging operations are performed across subjects; (ii) the global avgFC was also utilized in the baseline GCN; (iii) the final obtained FC matrices are further processed using the methods in “**Different graph processing meth-**

ods”, depicted in the right part of Figure 1.

- Different graph processing methods

To investigate the impact of different graph types on the classification results of GCN, we employ various processing methods to individual or global FC, as shown in the right part of Figure 1. In the first method, we take the k largest values in each row of the absolute FC matrix as the **k-NN graph**, as shown in Figure 1d. In the second method, we normalize the absolute FC values to the range $[0 - 1]$ for consistent thresholding, denoted as the normalized absolute FC (NAFC), and then the thresholding is applied on the NAFC matrix (denoted as **threshold graph**), as illustrated in Figure 1e.

2.2.3 Graph Convolutional Network (GCN)

Graphs (Zhou et al., 2020) represent a non-Euclidean data structure comprising nodes and edges, where nodes denote objects and edges signify relationships between these objects. Brain FC can be modeled as graphs, with nodes representing ROIs and edges corresponding to activity correlations between these ROIs (Hanik et al., 2022; Sporns et al., 2005; Suprano, 2019). GCNs (Scarselli et al., 2008; Micheli, 2009) have gained widespread popularity in machine learning for graph analysis, owing to their persuasive performance. The GCN architectures effectively integrate node features and graph topology to construct distributed node representations with graph convolutional layers (GCLs) (Errica et al., 2020). In this work, we introduce a novel GCN framework for binary classification of fMRI data, where the fMRI time series of brain ROIs are directly regarded as the node features and the FC serves as the graph topology.

- The Proposed GCN

The proposed GCN framework is implemented using the Pytorch Geometric (PyG) library (Fey and Lenssen, 2019). This library encompasses a variety of GNN models and graph preprocessing methods to easily build and train GNNs. The designed GCN framework, illustrated in Figure 2, comprises five GCLs based on GraphConv (Morris et al., 2019). The nonlinear activation function Rectified Linear Unit (ReLU) (Nair and Hinton, 2010) layer defined as $f(x) = \max(0, x)$ follows after each of the first 4 GCLs. The input of the last GCL layer is the outputs of the first 4 layers. The fifth GCL includes a batch normalization layer, enhancing the speed and stability of the GCN framework. Subsequently, the global mean pool or global average pool is followed to avoid overfitting and enhance the robustness of the framework. To further prevent overfitting, a dropout layer is implemented, randomly setting output data to zero with a specified probability.

In the presented GCN framework, the optimization is carried out using the Adam algorithm (Kingma and Ba, 2015), and the loss function employed is the cross-entropy loss. The proposed GCN framework is applied for two types of classification: one with global FC and the other with individual FC. For the classification with individual FC, as illustrated in Figure 2, the inputs consist of individual time series of ROIs with corresponding FC and labels. While, in the classification with global FC, the inputs of the GCN framework are individual time series of ROIs with the same global FC and labels of each sample.

- Baselines

For the purpose of comparison, we establish two baselines: the Support Vector Machine (SVM) employing the radial basis function (RBF) kernel (Burges, 1998), and the GCN architecture for fMRI analysis developed by Wang *et al.* (Wang et al., 2021) in 2021.

The baseline GCN architecture using avgFC consisted of 5 convolutional layers, one recurrent neural network (RNN) layer and a Softmax layer. In the original study, the GCN was applied for autism spectrum disorder (ASD) classification, attaining the best average accuracy of 70.7% (max 79.0%, min 66.7%) when $k = 3$ (among 3, 5, 10, and 20) using 10-fold cross validation.

2.2.4 Configurations

We reimplement the baseline GCN architecture and apply it to the OASIS-3 dataset using all recommended parameters from the original paper. In the current study, a 10-fold cross validation strategy is

adopted to evaluate the performance of the GCN framework which is set to be the same when applying the baseline GCN to OASIS-3 dataset.

Code of the proposed GCN framework is implemented based on Python, and the GCN structure is realized by PyTorch based on PyG. In our experiment, the output dimension of each convolutional layer is 128; the learning rate is set to 0.001; the dropout rate is set to 0.5; and the model is trained for 100 epochs with a batch size of 8.

To assess the impact of variations in the FC matrix on the outcomes, we varied the number of nearest neighbors k (1, 2, 3, and 4) and the threshold value (0.7, 0.8, 0.9, 0.95, and 0.99) for FC matrix processing. To evaluate the significant differences in classification results between the proposed GCN and the baseline GCN, as well as those between GCN with different types of FC, the independent t -test method was employed in this study. The brain networks of different global graphs in one fold are visualized with Brainnet viewer (Xia et al., 2013). The brain networks are grouped into seven canonical functional networks defined by the 7 Yeo networks (Buckner et al., 2011): visual network (VIS), somatomotor network (SMN), dorsal attention network (DAN), ventral attention network (VAN), limbic network (LIM), frontoparietal control network (FPC), default mode network (DMN).

3 RESULTS

As mentioned earlier, to better understand the impact of different FC, the proposed GCN utilizes the graphs of global FC (avgFC or FC-of-avgROI) or individual FC, and then the graphs are processed as k -NN graph and **threshold graph**, respectively. In this section, we provide the classification results for *MCI* vs. *NC* using GCN with k -NN graphs or threshold graph.

3.1 Results with k -NN Graph

We implement the *MCI* vs. *NC* classification of the proposed GCN with k -NN graphs obtained from individual FC, non-absolute individual FC, global FC of avgFC and FC-of-avgROI. Especially, we also utilize the non-absolute individual FC here to demonstrate the superiority of GCN with absolute FC over that with non-absolute FC. It should be noted that absolute FC are used as the default in this article. We compare the performance of our proposed GCN with the baseline GCN framework and SVM method. The experimental results are shown in Figure 3, which illustrates that:

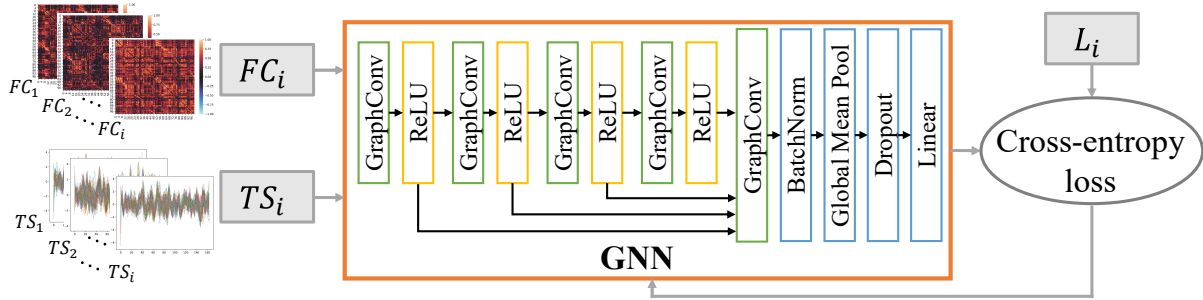


Figure 2: GCN classification with individual FC. TS_i denotes the i th individual time series of ROIs; FC_i and L_i denote the corresponding i th individual FC and label. In the classification with global FC, we utilize one same global FC for each individual time series of ROI.

1) The proposed GCN outperforms both the baseline GCN (best average accuracy of 68.6% when $k = 3$) and SVM (average accuracy of 56.8%) in terms of accuracy. The t -test outcomes in Table 1 show significant differences between the results of proposed GCN and the baseline GCN with different values of k at the 5% significance level. Our proposed GCN with k -NN graphs achieves the best average accuracy of 80.3% (max 87.3%, min 76.0%) with absolute-individual FC when $k = 1$.

2) The proposed GCN with k -NN graphs exhibits differently compared to the baseline GCN. While the accuracy of the baseline GCN increases as k increases and achieves the best average accuracy at $k = 3$ (the same as in ASD classification in the baseline paper), our proposed GCN's performance with individual or global FC declines as k increases.

3) The proposed GCN with absolute individual FC demonstrates a slight performance improvement compared to its counterpart with non-absolute individual FC.

4) Our proposed GCN with individual FC performs slightly better than that with global FC. The use of global avgFC or FC-of-avgROI exhibits negligible differences for the proposed GCN with k -NN graphs. Besides, the t -test results in Table 2 indicate that there are no significant differences between the outcomes of the individual and the two types of global FC across various values of k at the 5% significance level.

Brain networks of k -NN graphs of avgFC or FC-of-avgROI are displayed as Figure 4. It is important to note that the k -NN graphs are non-symmetrical matrices and cannot guarantee full connectivity. In this figure, there are only 50 and 45 edges in avgFC and FC-of-avgROI as $k = 1$, respectively. From the brain networks, it can be observed that:

1) Increasing k leads to more edges in both avgFC and FC-of-avgROI brain networks.

This highlights an important finding that excessive connectivity can have a detrimental effect on improving classification performance, which is evidenced by the diminishing performance results as the number of connectivity (k) increases.

2) The brain networks of k -NN avgFC and FC-of-avgROI show little difference for each value of k , which can explain the negligible difference of the accuracy between avgFC and FC-of-avgROI with the same k .

3) The brain networks of avgFC involve a slightly larger number of ROIs than FC-of-avgROI when $k = 1, 2$, and the average accuracy of GCN with avgFC are marginally higher than that of GCN with FC-of-avgROI. This finding illustrates that graphs involving a greater number of nodes may contain more valuable information for GCN classification.

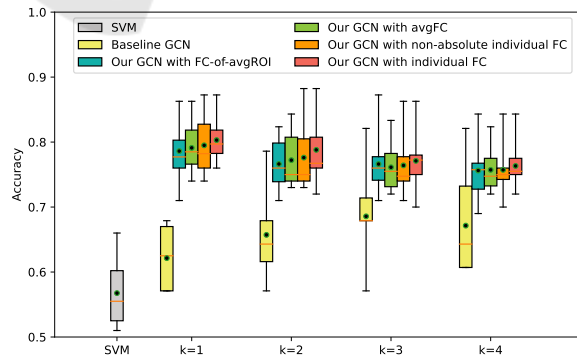


Figure 3: MCI vs. NC results of the proposed GCN framework with k -NN graph. The black dot in the box presents the average value in the 10-fold cross validation results.

Table 1: The probability results in t -test between baseline methods and our proposed GCNs with k -NN graph.

t -test	$k = 1$	$k = 2$	$k = 3$	$k = 4$
Baseline GCN vs. our GCN with individual FC	1.72×10^{-8}	5.19×10^{-5}	3.51×10^{-3}	2.97×10^{-3}
Baseline GCN vs. our GCN with avgFC	7.10×10^{-8}	1.20×10^{-4}	6.48×10^{-3}	4.43×10^{-3}
Baseline GCN vs. our GCN with FC-of-avgROI	3.32×10^{-7}	1.99×10^{-4}	5.43×10^{-3}	7.35×10^{-3}
SVM vs. our GCN with individual FC	4.47×10^{-10}	1.04×10^{-8}	1.87×10^{-8}	9.00×10^{-9}
SVM vs. our GCN with avgFC	1.54×10^{-9}	1.19×10^{-8}	1.80×10^{-8}	9.84×10^{-9}
SVM vs. our GCN with FC-of-avgROI	6.96×10^{-9}	1.73×10^{-8}	2.78×10^{-8}	5.73×10^{-8}

Table 2: t -test results between our proposed GCNs with k -NN graph of different types (individual, avgFC, FC-of-avgROI). P denotes the probability and CI denotes the confidence interval in the t -test.

t -test		avgFC vs. individual FC	FC-of-avgROI vs. individual FC	FC-of-avgROI vs. avgFC
$k = 1$	P	0.47	0.36	0.79
	CI	[-0.046,0.022]	[-0.055,0.021]	[-0.044,0.034]
$k = 2$	P	0.45	0.30	0.76
	CI	[-0.059,0.027]	[-0.064,0.021]	[-0.045,0.034]
$k = 3$	P	0.61	0.81	0.80
	CI	[-0.049,0.030]	[-0.047,0.037]	[-0.035,0.045]
$k = 4$	P	0.70	0.70	0.95
	CI	[-0.038,0.026]	[-0.045,0.031]	[-0.038,0.036]

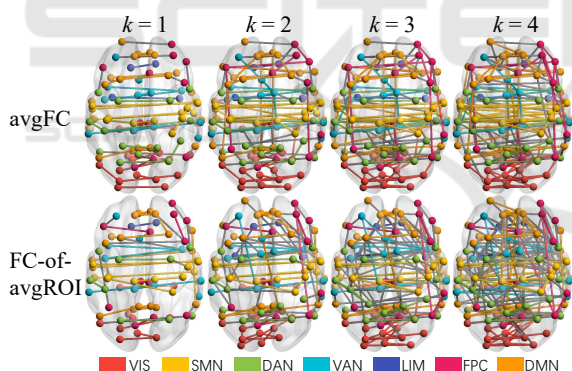


Figure 4: The brain networks of k -NN avgFC or FC-of-avgROI. The seven-colored nodes are indicative of seven grouped networks (VIS, SMN, DAN, VAN, LIM, FPC, DMN), while color-coded links denote self-network connectivity and grey links denote the between-network connectivity.

3.2 Results with Threshold Graph

The MCI vs. NC classification performances of the proposed GCN with threshold graph derived from individual FC, global FC of avgFC or FC-of-avgROI are reported in Figure 5. It can be observed that:

1) As the threshold value increases, the accuracy of GCN with FC-of-avgROI performs differently from that of GCN with individual FC or avgFC. The

t -test outcomes in Table 3 show significant differences between the results of the FC-of-avgROI and individual FC or avgFC with $threshold = 0.7, 0.8, 0.9$ or 0.95 at the 5% significance level

2) The average accuracy of GCN with FC-of-avgROI graphs are notably lower compared to that of GCN with individual FC or avgFC as $threshold \leq 0.95$, and then exhibits a significant rise when the threshold reaches 0.99.

3) The average accuracy of GCN with individual and avgFC graphs show a gradual increase and attain an optimal average accuracy at $threshold = 0.95$ and $threshold = 0.90$, respectively. Nonetheless, the accuracy of both decrease when $threshold = 0.99$.

4) In some cases (avgFC with all threshold values and FC-of-avgROI as $threshold = 0.99$), the GCN with global FC achieves comparable or even superior performance compared with GCN using individual FC. Moreover, the t -test outcomes in Table 3 indicate that there are no significant differences between the results of the individual and avgFC across various threshold values, and between the results of the individual and FC-of-avgROI as $threshold = 0.99$ at the 5% significance level. Overall, the proposed GCN with threshold graphs achieves the best average accu-

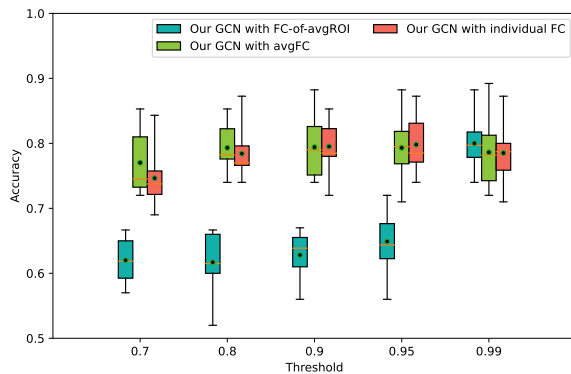


Figure 5: MCI vs. NC results of the proposed GCN framework with threshold graph.

accuracy of 80.0% (max 88.2%, min 74.0%) with FC-of-avgROI graphs when $threshold = 0.99$.

The brain networks of avgFC and FC-of-avgROI with different threshold values are displayed in Figure 6. It can be observed that:

1) Increasing threshold results in fewer edges in both networks. However, FC-of-avgROI contains much more edges than avgFC when $threshold > 0.7$. When few edges remain in the graph, there are self-network edges of SMN, DMN, FPC, and VIS in avgFC ($threshold = 0.9$ or $threshold = 0.95$); while, there are both self-network and between-network edges of SMN and VAN in FC-of-avgROI ($threshold = 0.99$).

2) The GCN with global FC that have very few edges in the graph obtained a higher average accuracy, which emphasizes the observation in k -NN graphs that excessive connectivity can negatively affect classification performance.

3) The slight decrease in average GCN accuracy with avgFC when there is only one edge left ($threshold = 0.99$) shows that a minimum number of edge information can cause a slight decrease in accuracy, although the ROI series contain a large amount of information. Furthermore, with suitable connectivity, the GCN with global FC can achieve comparable or superior performance compared with GCN with individual FC. These findings highlight the significance of suitable edge information for achieving performance, rather than the threshold itself.

4 DISCUSSION

In this study, we developed an FC based GCN framework for fMRI binary classifications to detect MCI

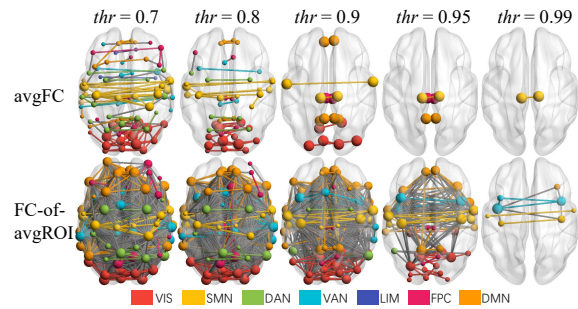


Figure 6: The brain networks of threshold avgFC or FC-of-avgROI. The size of nodes reflects the degree of the graph, and the nodes in k -NN graph have the same size. Other annotations are identical to Figure 4.

from NCs on the longitudinal OASIS-3 dataset. Besides, we explored the impact of different types and processing methods of FC on the GCN classification performance.

The results of our experiments revealed several important findings. First, our proposed GCN significantly outperformed both the baseline GCN and SVM in terms of accuracy, indicating its effectiveness for MCI diagnosis. The proposed GCN achieved the best average accuracy of 80.3% (11.7% higher than the baseline GCN and 23.5% higher than SVM) and the highest accuracy of 88.2%. This highlights the potential of deep learning techniques, specifically the GCN framework, for analyzing rfMRI data and detecting neurodegenerative disorders.

Second, we compared the effects of different types of FC utilized in the GCN. The proposed GCN with absolute individual FC performed slightly better than non-absolute individual FC. In this study, we found that the GCN framework with individual FC performed slightly better than that with global FC generally, which is consistent with most of the current studies (Parisot et al., 2017). This suggests that individual-specific FC may contain valuable information for classification tasks, and incorporating them into the GCN model can improve its performance. However, GCN using global graphs with appropriate connectivity can achieve equivalent or superior performance to individual graphs in some cases. This assertion is supported by t -test results indicating no significant differences between the individual and global FC in some cases at the 5% significance level.

Furthermore, we investigated different processing methods for FC matrices, including the k -NN graphs and threshold graphs. The results suggest that the choice of FC type and graph construction method can influence GCN classification performance. The GCN with k -NN graphs achieved the best average accuracy when k is set to 1, indicating that considering only the

Table 3: *t*-test results between our proposed GCNs with threshold graph of different types (individual, avgFC, FC-of-avgROI). *P* denotes the probability and *CI* denotes the confidence interval in the *t*-test.

<i>t</i> -test		avgFC vs. individual FC	FC-of-avgROI vs. individual FC	FC-of-avgROI vs. avgFC
<i>threshold</i> = 0.7	<i>P</i>	0.28	2.08×10^{-6}	3.04×10^{-7}
	<i>CI</i>	[-0.021,0.068]	[-0.165,-0.088]	[-0.190,-0.110]
<i>threshold</i> = 0.8	<i>P</i>	0.61	5.01×10^{-8}	3.94×10^{-8}
	<i>CI</i>	[-0.027,0.045]	[-0.207,-0.128]	[-0.217,-0.135]
<i>threshold</i> = 0.9	<i>P</i>	0.96	8.44×10^{-9}	4.85×10^{-8}
	<i>CI</i>	[-0.042,0.040]	[-0.202,-0.132]	[-0.205,-0.127]
<i>threshold</i> = 0.95	<i>P</i>	0.82	6.34×10^{-7}	4.76×10^{-6}
	<i>CI</i>	[-0.051,0.041]	[-0.191,-0.107]	[-0.191,-0.097]
<i>threshold</i> = 0.99	<i>P</i>	0.97	0.47	0.53
	<i>CI</i>	[-0.047,0.049]	[-0.028,0.057]	[-0.032,0.060]

nearest neighbors in the graph can be beneficial for classification.

Lastly, we analyzed the brain networks derived from the graphs used in the GCN framework. We observed that excessive connectivity or between-network connectivity in the networks could negatively impact the GCN classification performance. This discovery aligns with the current research status that few studies have demonstrated significant associations between disturbed self-network connectivity and cognitive impairments in MCI or AD (Huijser, 2021). The results indicate that the self-network connectivity in VIS, DMN, SMN, VAN and FPC may play a more significant role in GCN classification. These findings are in line with the findings in (Zheng et al., 2017) that disturbed FC of rest state was seen in the DMN and VIS in AD patients. Li et al. (2015) found that both MCI and AD patients showed hyperactivation fell in frontoparietal, VAN, DMN and SMN relative to NCs. Katsumi et al. (2023) observed that increased baseline atrophy in the FPC and DMN was related to a higher risk of progression to dementia.

5 CONCLUSIONS

In this study, we formulated an FC based GCN framework for binary classifications of fMRI data. Specifically, we applied this framework for the detection of MCI from NCs using the longitudinal OASIS-3 dataset. Additionally, we systematically explored the influence of various FC types (individual FC, avgFC, FC-of-avgROI) and processing methods (*k*-NN and threshold) on the GCN classification performance. The proposed GCN framework exhibits significantly superior performance compared with the baseline GCN and SVM. The outcomes of our investigation offer valuable insights into the applica-

tion of FC-based graphical approaches in brain analysis and disease detection. These findings significantly contribute to the understanding of neurodegenerative disorders, presenting potential clinical applications in the detection and management of neurodegenerative diseases, particularly in the context of MCI or AD. and potential clinical applications in MCI or AD detection and management of neurodegenerative diseases. Further research can explore additional FC measures and refine the GCN framework to improve classification performance and expand its applicability in clinical settings.

ACKNOWLEDGEMENTS

This work was carried out as part of the doctoral program in Experimental Sciences and Technology at the University of Vic - Central University of Catalonia. F.D. work was supported in part by the Tianjin Science and Technology Plan Project (No. 22PTZWHZ00040). C.F.C work was partially supported by grants PICT 2020-SERIEA-00457 and PIP 112202101 00284CO (Argentina). J.S.-C. work was partially supported by the University of Vic-Central University of Catalonia grant R0947.

REFERENCES

- Avants, B. B., Epstein, C. L., Grossman, M., and Gee, J. C. (2008). Symmetric diffeomorphic image registration with cross-correlation: evaluating automated labeling of elderly and neurodegenerative brain. *Medical image analysis*, 12(1):26–41.
- Bi, X., Zhao, X., Huang, H., Chen, D., and Ma, Y. (2020). Functional brain network classification for Alzheimer’s disease detection with deep features and

- extreme learning machine. *Cognitive Computation*, 12(3):513–527.
- Buckner, R. L., Krienen, F. M., Castellanos, A., Diaz, J. C., and Yeo, B. T. (2011). The organization of the human cerebellum estimated by intrinsic functional connectivity. *Journal of neurophysiology*, 106(5):2322–2345.
- Bullmore, E. and Sporns, O. (2009). Complex brain networks: graph theoretical analysis of structural and functional systems. *Nature Reviews Neuroscience*, 10(3):186–198.
- Burges, C. J. (1998). A tutorial on support vector machines for pattern recognition. *Data mining and knowledge discovery*, 2(2):121–167.
- Chandra, A., Dervenoulas, G., and Politis, M. (2019). Magnetic resonance imaging in Alzheimer’s disease and mild cognitive impairment. *Journal of Neurology*, 266(6):1293–1302.
- Chen, X., Li, B., Jia, H., Feng, F., Duan, F., Sun, Z., Cai, C. F., and Solé-Casals, J. (2022). Graph empirical mode decomposition-based data augmentation applied to gifted children MRI analysis. *Frontiers in Neuroscience*, 16:866735.
- Errica, F., Podda, M., Bacciu, D., and Micheli, A. (2020). A fair comparison of graph neural networks for graph classification. In *International Conference on Learning Representations (ICLR 2020)*.
- Esteban, O., Markiewicz, C. J., Blair, R. W., Moodie, C. A., Isik, A. I., Erramuzpe, A., Kent, J. D., Goncalves, M., DuPre, E., Snyder, M., et al. (2019). fMRIPrep: a robust preprocessing pipeline for functional MRI. *Nature methods*, 16(1):111–116.
- Fey, M. and Lenssen, J. E. (2019). Fast graph representation learning with PyTorch Geometric. In *ICLR Workshop on Representation Learning on Graphs and Manifolds*.
- Greve, D. N. and Fischl, B. (2009). Accurate and robust brain image alignment using boundary-based registration. *Neuroimage*, 48(1):63–72.
- Han, S., Sun, Z., Zhao, K., Duan, F., Cai, C. F., Zhang, Y., and Solé-Casals, J. (2024). Early prediction of dementia using fMRI data with a graph convolutional network approach. *Journal of Neural Engineering*. Submitted, under review.
- Hanik, M., Demirtaş, M. A., Gharsallaoui, M. A., and Rekić, I. (2022). Predicting cognitive scores with graph neural networks through sample selection learning. *Brain Imaging and Behavior*, 16(3):1123–1138.
- Huijser, D. (2021). Functional connectivity changes and cognitive deficits in Alzheimer’s disease: A review.
- Katsumi, Y., Quimby, M., Hochberg, D., Jones, A., Brickhouse, M., Eldaief, M. C., Dickerson, B. C., and Touroutoglou, A. (2023). Association of regional cortical network atrophy with progression to dementia in patients with primary progressive aphasia. *Neurology*, 100(3):e286–e296.
- Kingma, D. P. and Ba, J. L. (2015). Adam: A method for stochastic optimization. pages 1–13.
- LaMontagne, P. J., Benzinger, T. L., Morris, J. C., Keefe, S., Hornbeck, R., Xiong, C., Grant, E., Hassenstab, J., Moulder, K., Vlassenko, A. G., et al. (2019). OASIS-3: longitudinal neuroimaging, clinical, and cognitive dataset for normal aging and Alzheimer’s disease. *MedRxiv*.
- Li, H.-J., Hou, X.-H., Liu, H.-H., Yue, C.-L., He, Y., and Zuo, X.-N. (2015). Toward systems neuroscience in mild cognitive impairment and Alzheimer’s disease: A meta-analysis of 75 fMRI studies. *Human brain mapping*, 36(3):1217–1232.
- Liu, F., Zhang, Y., Rekić, I., Massoud, Y., and Solé-Casals, J. (2022). Graph learning for brain imaging. *Frontiers in Neuroscience*, 16:1001818.
- Liu, S., Cai, W., Liu, S., Zhang, F., Fulham, M., Feng, D., Pujol, S., and Kikinis, R. (2015). Multimodal neuroimaging computing: a review of the applications in neuropsychiatric disorders. *Brain Informatics*, 2(3):167–180.
- Micheli, A. (2009). Neural network for graphs: A contextual constructive approach. *IEEE Transactions on Neural Networks*, 20(3):498–511.
- Morris, C., Ritzert, M., Fey, M., Hamilton, W. L., Lenssen, J. E., Rattan, G., and Grohe, M. (2019). Weisfeiler and leman go neural: Higher-order graph neural networks. In *Proceedings of the AAAI Conference on Artificial Intelligence*, volume 33, pages 4602–4609.
- Nair, V. and Hinton, G. E. (2010). Rectified linear units improve restricted boltzmann machines. In *ICML*.
- Parisot, S., Ktena, S. I., Ferrante, E., Lee, M., Moreno, R. G., Glocker, B., and Rueckert, D. (2017). Spectral graph convolutions for population-based disease prediction. In *International Conference on Medical Image Computing and Computer-assisted Intervention*, pages 177–185. Springer.
- Pruim, R. H., Mennes, M., van Rooij, D., Llera, A., Buitelaar, J. K., and Beckmann, C. F. (2015). Ica-aroma: A robust ica-based strategy for removing motion artifacts from fMRI data. *Neuroimage*, 112:267–277.
- Qu, Z., Yao, T., Liu, X., and Wang, G. (2023). A graph convolutional network based on univariate neurodegeneration biomarker for Alzheimer’s disease diagnosis. *IEEE Journal of Translational Engineering in Health and Medicine*.
- Scarselli, F., Gori, M., Tsoi, A. C., Hagenbuchner, M., and Monfardini, G. (2008). The graph neural network model. *IEEE Transactions on Neural Networks*, 20(1):61–80.
- Schaefer, A., Kong, R., Gordon, E. M., Laumann, T. O., Zuo, X.-N., Holmes, A. J., Eickhoff, S. B., and Yeo, B. T. (2018). Local-global parcellation of the human cerebral cortex from intrinsic functional connectivity MRI. *Cerebral cortex*, 28(9):3095–3114.
- Sporns, O., Tononi, G., and Kötter, R. (2005). The human connectome: a structural description of the human brain. *PLoS computational biology*, 1(4):e42.
- Srivastava, S., Ahmad, R., and Khare, S. K. (2021). Alzheimer’s disease and its treatment by different approaches: A review. *European Journal of Medicinal Chemistry*, 216:113320.
- Suprano, I. (2019). *Cerebral connectivity study by func-*

- tional and diffusion MRI in intelligence*. PhD thesis, Université de Lyon.
- Tang, H., Ma, G., Guo, L., Fu, X., Huang, H., and Zhan, L. (2022). Contrastive brain network learning via hierarchical signed graph pooling model. *IEEE Transactions on Neural Networks and Learning Systems*.
- Wang, L., Li, K., and Hu, X. P. (2021). Graph convolutional network for fMRI analysis based on connectivity neighborhood. *Network Neuroscience*, 5(1):83–95.
- Xia, M., Wang, J., and He, Y. (2013). Brainnet viewer: a network visualization tool for human brain connectomics. *PloS one*, 8(7):e68910.
- Zhang, Y., Brady, J. M., and Smith, S. (2000). Hidden markov random field model for segmentation of brain mr image. In *Medical Imaging 2000: Image Processing*, volume 3979, pages 1126–1137. SPIE.
- Zheng, W., Liu, X., Song, H., Li, K., and Wang, Z. (2017). Altered functional connectivity of cognitive-related cerebellar subregions in Alzheimer’s disease. *Frontiers in aging neuroscience*, 9:143.
- Zhou, J., Cui, G., Hu, S., Zhang, Z., Yang, C., Liu, Z., Wang, L., Li, C., and Sun, M. (2020). Graph neural networks: A review of methods and applications. *AI Open*, 1:57–81.

